Terahertz mirage: Deflecting terahertz beams in an inhomogeneous artificial dielectric based on a parallel-plate waveguide

Rajind Mendis, Jingbo Liu, and Daniel M. Mittleman
Department of Electrical and Computer Engineering, MS-378, Rice University, Houston, Texas 77251, USA

(Received 3 April 2012; accepted 29 August 2012; published online 12 September 2012)

The field of metamaterials and the formalism of transformation optics have provided a prescription for constructing artificial dielectrics with unique properties such as light trapping and cloaking. Here, we describe a different approach to creating an inhomogeneous artificial medium, based on waveguide techniques, which does not rely on engineered subwavelength-scale components. We demonstrate a mirage effect in which an object several times larger than the selected wavelength is rendered invisible by bending a beam around it. © *2012 American Institute of Physics*. [http://dx.doi.org/10.1063/1.4752241]

Transformation optics is a conceptual approach for designing a medium to control the flow of electromagnetic waves in counter-intuitive ways.[1] Together with the ideas of metamaterials,[2,3] this provides a prescription for constructing artificial dielectrics with unique capabilities such as light trapping[4,5] and cloaking,[3,6] which would otherwise be difficult to achieve. Of course, the idea of an artificial dielectric medium dates back over 50 years to the use of metal waveguides for lensing,[7,8] but the versatility of this older approach in forming an *inhomogeneous* dielectric has not been appreciated. Here, we show that a waveguide-based strategy can also be used to create a medium with an inhomogeneous effective dielectric constant. Using this technique, we demonstrate a mirage effect which can be used to hide an object several times larger than the free-space wavelength, at terahertz (THz) frequencies. This approach offers many of the same intriguing possibilities as that of metamaterials and transformation optics, except that the wave propagates in air rather than inside a solid[9] or in an array of subwavelength structures.[2,3] As a result, the dielectric function is truly continuous in space, and the propagation path of the wave is experimentally accessible. This approach is well suited to the THz range, where there is a compelling need for new and versatile techniques for manipulating wave propagation.[10] In addition, it may be more readily translated to shorter wavelengths than those based on sub-wavelength-scale engineering.[11]

The use of waveguide-based artificial dielectrics, although first studied in the 1940 s in the microwave region,[7] never became popular because such structures were unreasonably large and unwieldy for practical use. We have recently revisited these ideas for applications in the THz region,[12,13] where the wavelength scaling permits structures of a more manageable size. Similar ideas have recently been proposed for cloaking at optical frequencies.[6] Our approach is based on the characteristic frequency dependence in the phase velocity of the TE_1 mode of the parallel-plate waveguide (PPWG). This medium exhibits an effective refractive index given by $n_{eff} = \sqrt{1 - (c/2bf)^2}$, where b is the plate separation, f is the frequency, and c is the free-space velocity of light. This indicates that the index n_{eff} can be tuned between zero and unity, either by varying the frequency for a given plate separation or by varying the plate separation for a given frequency.

In this report, we discuss the use of this concept to form an *inhomogeneous* two-dimensional artificial dielectric medium. A key aspect of the approach described here is the ability to engineer the index continuously in two dimensions. Continuous variation of the index in an artificial dielectric is difficult to achieve in many experimental situations, since one often relies on homogenization of arrays of subwavelength structures.[9] In our case, one may create a desired refractive index profile $n_{eff}(x,y)$ by choosing the plate separation $b(x,y)$ appropriately. This approach is effective as long as the change in plate spacing is *adiabatic* with respect to the wavelength, so that the single-mode nature of the input wave is preserved.[6]

To validate this concept, we first consider the simple case where the index varies monotonically along just one spatial dimension. Starting from the conventional PPWG geometry, this can be achieved by inclining one plate with respect to the other such that the plate separation varies along the dimension perpendicular to the propagation axis. In general, light rays propagating inside an inhomogeneous dielectric medium will bend towards the high-index region, an effect which is familiar in the analysis of mirages and GRIN (gradient-index) lenses. Therefore, we expect a THz beam propagating inside the waveguide to bend towards the region of larger plate separation, even though the medium between the two plates is simply air.

For this experiment (inset of Fig. 1), broadband THz pulses are coupled into the waveguide at normal incidence, with the electric field polarized to excite the TE_1 mode. The position of the input optic axis is chosen as the spatial reference ($x = 0$) along the width of the waveguide, at which point the plate separation is 0.75 mm. The top plate is angled by $\theta = 0.72°$ with respect to the bottom plate, such that the plate separation increases towards the positive x direction. The length of the plates along the input optic axis is 1 cm. Output signals are detected at various points along the x direction, 3 cm from its output face, using a fiber-coupled THz receiver.

The calculated refractive index profiles for this waveguide geometry at several frequencies are given in Fig. 1. These curves indicate that for a given waveguide width, the index gradient decreases, as the frequency increases. As in

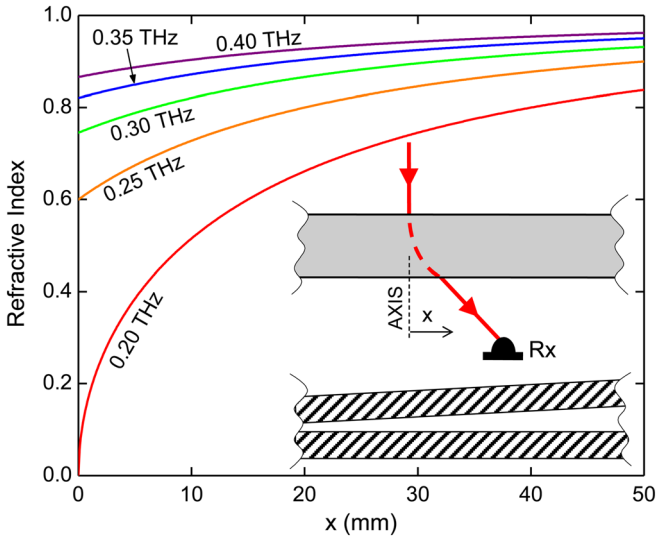

FIG. 1. Calculated refractive index profiles, as a function of the transverse (x) coordinate, for several different frequencies. The inset illustrates a plan view of the experimental schematic and a cross-section of the waveguide. The path of the THz beam is indicated by the (red) ray. The inclination of the top plate is exaggerated for clarity.

the case of a mirage, we expect that a larger index gradient would result in a higher degree of beam bending. This implies that the output beams corresponding to the low-frequency (LF) components of the input broadband pulse should experience a greater deflection than the high-frequency (HF) components. The detected output signals for four different receiver positions and their corresponding amplitude spectra are shown in Figs. 2(a) and 2(b), respectively. The signals indicate a negative chirp where the HF components arrive earlier in time, characteristic of the TE_1 mode. The predicted beam-bending behavior is more apparent in the spectra. They indicate a progressive attenuation of the HF components and a progressive build-up of LF components, as the receiver is moved away from the optic axis (in the $+x$ direction). In fact, far away from the optic axis, we observe LF components that are not present in the on-axis signal. This implies that the LF components of the input pulse are bending more than the HF components.

We can extract the spectral amplitude component at each position of the receiver and map the frequency-dependent spatial intensity profiles of the output beam. These are presented in Fig. 3(a) by the red dotted curves for three specific frequencies to illustrate the results. For comparison, we have also plotted the corresponding measurements (black dotted curves) when the plates are perfectly parallel to each other as in a conventional PPWG. The black curves are all centered at $x = 0$, indicating no beam deflection. However, the red curves show a very clear shift towards the $+x$ direction, increasing as the frequency decreases. These intensity profiles can be used to quantify the beam deflection by extracting the shift in the *centroid* of the profiles. This frequency-dependent displacement from the input axis is plotted in Fig. 3(b), for three different input coupling positions of the beam. To confirm our understanding of this behavior, we simulate the problem using a numerical ray tracing calculation. The inhomogeneous medium is modeled by calculating the index profile for each frequency. These

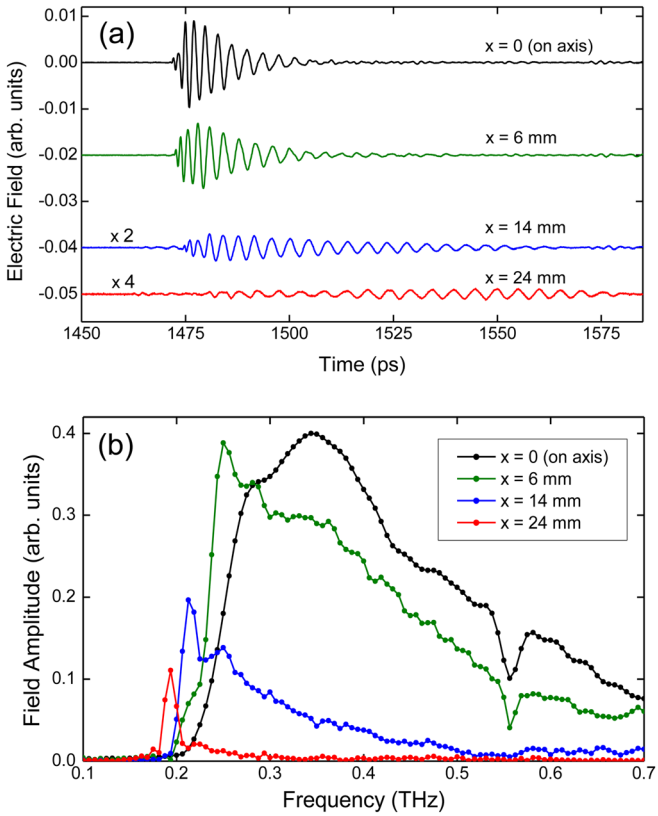

FIG. 2. Detected output signals (a), and their Fourier-transformed amplitude spectra (b), for four different receiver positions. The black, green, blue, and red curves correspond to the positions when the receiver is (looking) on axis, 6 mm, 14 mm, and 24 mm away from axis, respectively.

results [solid curves in Fig. 3(b)] show good agreement with the measurements. The deviations are probably caused by the finite extent of the measured profiles, since the simulated results are based on a single ray of infinitesimal lateral extent, while the detector has a relatively large (6 mm) collection aperture. Nevertheless, this result demonstrates that a wave propagating in the TE_1 mode experiences the empty space between the plates as if it were a dielectric with a continuously varying refractive index (less than unity).

Using more sophisticated designs, more elaborate control of beam propagation is possible. Next, we explore a possible approach to bending a light beam around an obstructing object. This is the essence of a mirage and is similar to recent examples of electromagnetic cloaking.[3,14] The design relies on a "roof" structure, where the upper waveguide plate has two complementary flat inclined surfaces [Fig. 4(a)]. In this case, the plate separation b varies with the transverse coordinate as $b(x) = b_0 - m|x|$, where b_0 is the maximum plate separation (at $x = 0$, the roof apex) and m is the slope of the roof. Fig. 4(b) shows the results of a ray-tracing calculation for two rays (corresponding to two different input frequencies), propagating into and through the waveguide. For a ray at the design frequency (red ray), the ray loops around the location of a hypothetical obstruction, and so the output beam is unaffected by the presence or absence of this obstruction, appearing to pass straight through the waveguide with minimal deviation. At a different frequency (blue ray), the ray passes through the location of the obstruction, so it should cast a shadow.

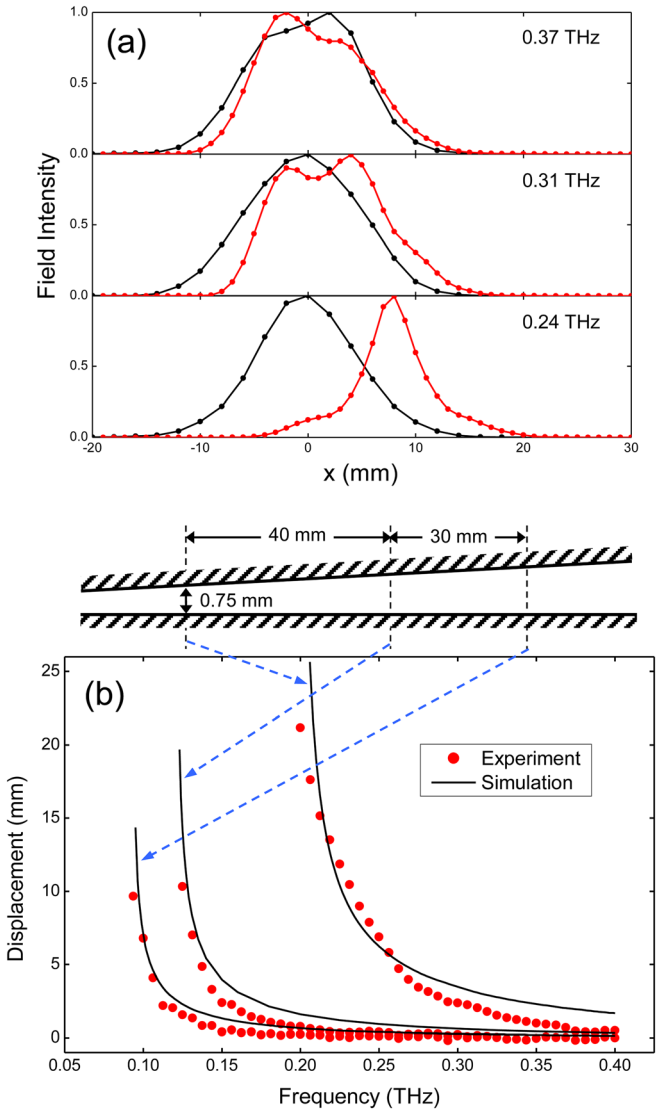

FIG. 3. (a) Intensity profiles of the output beam for three representative frequencies, measured 3 cm away from the output face of the waveguide. The red curves correspond to the case depicted in the inset of Fig. 1, where the top plate is inclined. The black curves correspond to the case when the plates are perfectly parallel to each other. (b) Beam displacement as a function of frequency, for three different input coupling positions, extracted from data like those shown in (a). The respective input coupling positions are indicated by the cross-sectional diagram shown above the figure. The red dots are experimental and the solid black curves are the results of a numerical simulation.

To confirm the expected behavior, we also perform full three-dimensional numerical simulations of the experiments (described below) using the finite element method.[15] Fig. 4(c) shows a cross-section of one simulation, in a plane through the middle of the gap between the two waveguide plates. In this simulation, a metallic obstruction (the object to be hidden) is included inside the waveguide. The curved path of the normally incident light wave avoids the obstruction and emerges from the waveguide unaffected by its presence. This is confirmed by Figs. 4(d) and 4(e), which show that the intensity patterns at the output facet of the waveguide, with and without the metal obstruction in the beam path, are almost indistinguishable.

For an experimental validation of this mirage, we choose a waveguide with a length (along the input optic axis) of 5 cm. The mirror plane (at $x = 0$) is located 9.2 cm

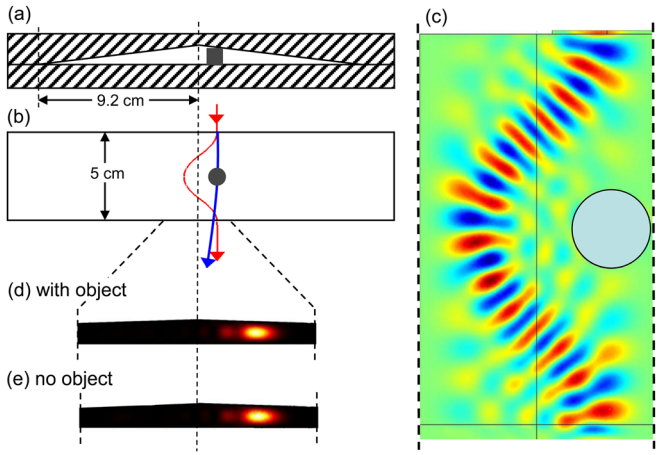

FIG. 4. (a) A cross-sectional view of the waveguide showing the roof-apex shape of the guiding region, with a cylindrical object inserted inside to one side of the apex location ($x = 0$). (b) Plan view of the structure, showing the cylindrical object (centered from the input and output faces) as a gray circle. The red and blue curves are numerically computed ray paths for the experimental configuration. The red ray corresponds to 0.16 THz, the design frequency, while the blue ray corresponds to 0.54 THz, far from the design frequency. (c) A finite-element-method simulation of the experimental geometry, showing the wave path inside the waveguide, as well as the hidden object. Panels (d) and (e) show the simulated intensity pattern at the output facet of the waveguide, with and without the object in place. Dimensions are not to scale.

from the plate-contact axis, and the inclination angle is 0.68°. The design frequency is chosen to be 0.16 THz. The object is a solid metallic circular disk with a 10 mm diameter (corresponding to more than 5λ), located on the optic axis of the input beam, 16 mm to one side of the waveguide apex. Similar to the previous experiment, the receiver is scanned 3 cm away from the output face to map the output beam profiles, in this case both with and without the object placed inside the waveguide. The measured intensity profiles at two

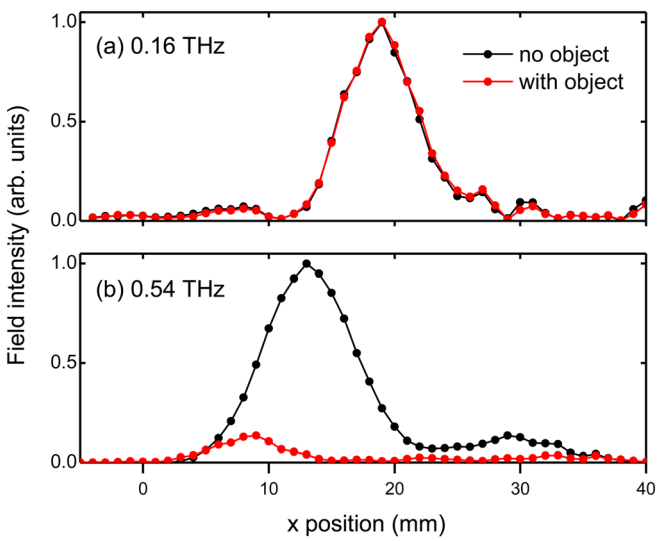

FIG. 5. Comparisons of the experimentally measured output intensity profiles with and without the object inside the waveguide. (a) The intensity patterns at the design frequency of 0.16 THz, and (b) the patterns at a frequency of 0.54 THz. The efficacy of the device at its design frequency is evident from the fact that the output beam profile is unaffected by the presence of the metal object inside the waveguide, even though it is situated on the optic axis of the input beam.

different frequencies are shown in Fig. 5. At the design frequency [Fig. 5(a)], the presence of the obstruction is impossible to detect, since the two curves are almost identical. At a different frequency [Fig. 5(b)], the obstruction lies squarely in the beam path, and therefore has a large effect on the output beam profile.

In conclusion, we demonstrate the use of waveguide-based artificial dielectrics to form inhomogeneous dielectric media in the THz regime. As a result, we can engineer the effective refractive index experienced by a propagating wave in two dimensions, to be in the range $0 < n(x,y) < 1$. It is possible to bend the paths of light beams around an obstruction, even though they are propagating in air. This permits us to effectively hide a metal object with a size larger than the wavelength. Unlike other recent strategies for controlling the path of a beam, where the inhomogeneous dielectric is either a solid[9] or a microstructured medium,[2,3] this approach gives us the ability to have experimental/physical access to the region of space in which the beam propagates, where the effective index is a continuously varying function. Furthermore, since this strategy does not require the use of subwavelength-scale engineered components, it may be more readily generalizable to shorter wavelengths. For completeness, we note that the functionality of the demonstrated device depends on the proper choice of input polarization, normal incidence of the input beam, and the proper choice of input coupling position for a given design frequency.

[1]A. V. Kildishev, W. Cai, U. K. Chettiar, and V. M. Shalaev, New J. Phys. **10**, 115029 (2008).
[2]D. R. Smith, J. B. Pendry, and M. C. K. Wiltshire, Science **305**, 788 (2004).
[3]D. Schurig, J. J. Mock, B. J. Justice, S. A. Cummer, J. B. Pendry, A. F. Starr, and D. R. Smith, Science **314**, 977 (2006).
[4]E. E. Narimanov and A. V. Kildishev, Appl. Phys. Lett. **95**, 041106 (2009).
[5]M. S. Jang and H. Atwater, Phys. Rev. Lett. **107**, 207401 (2011).
[6]I. I. Smolyaninov, V. N. Smolyaninova, A. V. Kildishev, and V. M. Shalaev, Phys. Rev. Lett. **102**, 213901 (2009).
[7]W. E. Kock, Proc. IRE **34**, 828 (1946).
[8]J. Brown, Proc. IEE **100**, 51 (1953).
[9]T. Zentgraf, Y. Liu, M. H. Mikkelsen, J. Valentine, and X. Zhang, Nat. Nanotechnol. **6**, 151 (2011).
[10]D. P. Gaillot, C. Croenne, and D. Lippens, Opt. Express **16**, 3986 (2008).
[11]M. G. Silveirinha, A. Alu, and N. Engheta, Phys. Rev. B **78**, 075107 (2008).
[12]R. Mendis and D. M. Mittleman, IEEE Trans. Microwave Theory Tech. **58**, 1993 (2010).
[13]R. Mendis, A. Nag, F. Chen, and D. M. Mittleman, Appl. Phys. Lett. **97**, 131106 (2010).
[14]U. Leonhardt and T. Tyc, Science **323**, 110 (2009).
[15]J. Deibel, M. Escarra, N. Berndsen, K. Wang, and D. M. Mittleman, Proc. IEEE **95**, 1624 (2007).